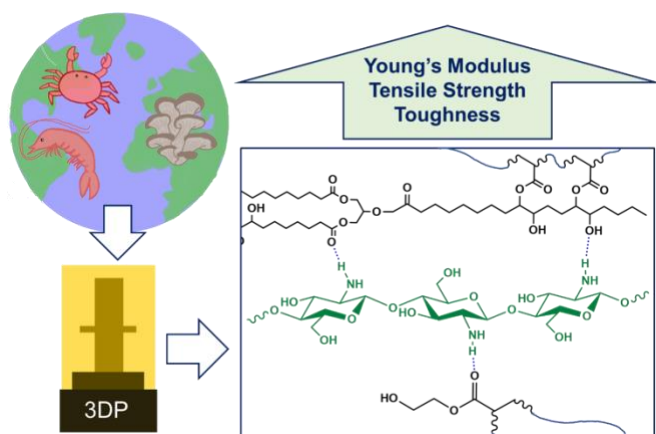


# The Effects of Chitosan Source on the Properties of 3D Printed Polymer Composites

Lyndsay C. Ayers<sup>1</sup>, Rebecca M. Johnson<sup>1</sup>, Ariel R. Tolfree<sup>1</sup>, Noora M. Al Kharji<sup>1</sup>, Milinda C. Senarathna<sup>1</sup>, Niyati Arora<sup>1</sup>, Ronald A. Smaldone<sup>1\*</sup>

\*Email: ronald.smaldone@utdallas.edu

<sup>1</sup>Department of Chemistry and Biochemistry, The University of Texas at Dallas, 800 W. Campbell Rd. Richardson, Texas, 75080, USA



## Abstract

Chitosan, or deacetylated chitin, is a linear polysaccharide composed of glucosamine and N-acetyl glucosamine units. Chitin is found in the cell walls of crustaceans, fungi, and insects, making chitosan the second most abundant natural polymer on earth. The broad availability of chitosan makes it an attractive material for applications in the textile, medical, and agricultural industries as well as for use in environmental waste remediation. Additive manufacturing, or 3D

printing, is a technique that can be used to produce polymeric materials on demand, based on custom digital designs. Using a digital light projection (DLP) 3D printer, we incorporated chitosan from different sources into photoresins, considering different sources for their sustainability. We explored how the source of the chitosan (fungal vs. crustacean) can affect the mechanical properties, resin incorporation, and printability of the photoresin. The 3D printed materials were tested to compare the mechanical properties of the polymers with chitosan from different sources. Higher loadings of chitosan improved the strength of the printed materials. We show that chitosan with higher loading and higher molecular weights improved the mechanical properties. However, the source of the chitosan affected the incorporation and printability of the photoresins.

## Keywords

3D Printing, Chitosan, Bioplastics, Additive manufacturing, Digital Light Projection Printing

# 1. Introduction

The creation of synthetic plastics has many benefits – and drawbacks. While plastic is an extremely versatile material, it has a problematic impact on the environment. It is estimated that millions of tons of mismanaged plastic end up in the ocean every year. Most plastics are made using non-renewable petroleum-based feedstocks and additives. Plastic is a common commodity material used in food packaging, household items, and many single use applications which are a major source of pollution with single use plastic greatly dominating the source of litter. One way to change this is by aiming to find sustainable alternatives and create eco-friendlier materials with similar, if not better, properties.

Using the process of additive manufacturing (also known as 3D printing) we can use customized computer aided designs (CAD) to transform plastic filaments or liquid resins to physical objects.<sup>1–7</sup> This method allows us to forego conventional molds or subtractive manufacturing methods, both of which result in environmental waste. Another benefit of 3D printing is that it allows for onsite production, which can reduce cost and energy consumption related to transportation and production time.<sup>1,8</sup> Digital light projection (DLP) 3D printing technology uses a projected light source to create high resolution prints compared to filament 3D printing.<sup>1,2,6</sup> There are, however, a limited number of bio-based resin formulations successfully used in industrial manufacturing, due to a lack in strength and functionality.<sup>8–12</sup> A solution to this issue is to use composite resins, which can improve the functionality and performance of the material.<sup>8,10–12</sup> One major design obstacle is in creating homogenous photorecins that are compatible with DLP and are within a printable viscosity range (~50 cps). With higher composite filler loadings there is a risk of separation, high resin viscosity, voids and defects, and filler clumping, all of which can impact quality of the printed objects.<sup>8</sup> Different types of composites can be used to improve various thermoset materials through mechanical properties, thermal stability, and biodegradability.<sup>8,10–12</sup>

Carbohydrate and cellulose-based fillers are gaining attention in polymer and 3D printing composite design as they are naturally-sourced and can have diverse structure, chemical functionality and morphology.<sup>13–15</sup> Chitosan, also known as deacetylated chitin, is a linear polysaccharide composed of both glucosamine and N-acetyl glucosamine units.<sup>16–28</sup> Chitin acts as a structural material that resides in the cell walls of crustaceans, fungi, algae, and insects.<sup>16–19,21–23,29</sup> This cellulose-like biopolymer is the second most abundant natural polymer on Earth.<sup>3,18–23</sup> The source of chitin changes the distribution pattern and mole fraction of the D-glucosamine residues present.<sup>21</sup> Additionally, chitin from animal sources may contain bound amino acid residues from complex proteins of the animal, while the fungal chitin will not contain proteins but other polysaccharides.<sup>18,21</sup> Both crustacean and mushroom chitin require extra steps to isolate and deacetylate the desired biopolymer. Chitin's wide availability has made it an attractive material for applications in agriculture, medical, and textile industries as well as for use in environmental water waste remediation.<sup>4–7,18,21,23,30</sup>

Crustacean chitin is often obtained as a byproduct of the fishing industry with the goal of reallocating waste.<sup>19</sup> While naturally prolific, chitin it is not always readily accessible for use as a scalable commodity material.<sup>17,18,21</sup> The amount available from crustaceans is restricted based on market demands and fishing regulations.<sup>18,31,32</sup> In addition to market restrictions, this form of chitin cultivation can contribute to marine animal habitat and population damage.<sup>31</sup> For example, due to declining crab populations in the Alaskan arctic, commercial fishing has been closed for the 2022-

2024 seasons.<sup>31</sup> As ocean acidification and crustacean population numbers will continue to be an issue, obtaining chitin from these sources will become increasingly problematic.

As an alternative, chitin and chitosan can be obtained from plant-based sources such as mushrooms. Fungal sources contain less chitin by weight than marine sources, however, there are fungal sources with potential for the direct commercial production of chitosan.<sup>16,19,21,23</sup> There are ways to increase the global fungal chitosan production by growing the mushrooms in a lab using inexpensive growing mediums, using waste from fungal biomasses, and by fermentation.<sup>24–28,33</sup> For instance, the antibiotic penicillin, produced from the *penicillium* species, creates 1.2 million tons of *penicillium* mycelial biomass biowaste a year with a potential recovery of roughly 57 grams of chitosan per kilogram of biomass.<sup>24,32,33</sup> These industries produce thousands of tons of fungi biomass a year that could be used to increase the amount of commercially viable chitosan. Another advantage of using fungal sourced chitosan is that they are hypoallergenic.<sup>23</sup> Mushrooms sourced chitin does not contain allergenic proteins like tropomyosin, which is often found in the shell of crustaceans.<sup>23</sup>

In this work, we explore the effects of chitosan as an additive into DLP 3D-printed photoresins. These resins include the bio-based monomer acrylated epoxidized soybean oil to improve the suspension of the chitosan and also offset the use of petroleum-based materials. Despite the wide availability of chitin and the ease of producing chitosan, designing chitosan-based composites is impeded due to the lack of fundamental knowledge of the composition-structure-property relationships for these materials, especially for newer, non-crustacean sourced chitosans.<sup>17</sup>

## 2. Experimental

### 2.1 Materials

All chemicals were used as received unless otherwise noted. 2-hydroxyethyl acrylate (HEA) and chitosan (CCBM) (5-20 mPa • s, 0.5% in 0.5% acetic acid at 20 °C) was purchased from TCI. Soybean oil, epoxidized acrylate (AESO) (CAS 91722-14-4), chitosan (CC) (CAS 9012-76-4), and phenylbis (2,3,6-trimethylbenzoyl) phosphine oxide (BAPO >96%) were purchased from Sigma-Aldrich. Mushroom chitosan 400cps (MC400) (product GBS002), 600cps (MC600) (product GBS003), and oligosaccharide (MCO) (product GBS005) was provided by Chibio Biotech.

### 2.2 Preparation of Photoresins

All chitosans were used as obtained, except CCBM (5-20mPa • s, 0.5% in 0.5% acetic acid at 20 °C), as the large chitosan particles could not be incorporated into the resins without modification. To overcome this, CCBM chitosan was ground in a mini-planetary ball mill model PMV1-0.4L. A 50mL stainless steel grinding jar and stainless-steel balls with 10 mm diameter were used in this experiment. CCBM (4 g, 5-20mPa • s, 0.5% in 0.5% acetic acid at 20 °C) was placed in the grinding jar and milled at 870 RPM for 6.5 h to produce a fine-powder morphology. To prepare a 30mL sample of resin, the monomer 2-HEA and crosslinker AESO were used in a 25:75 by weight ratio, respectively. To an amber vial, AESO (7.5g) and 2-HEA (22.5g) were added.

The vial was then gently warmed using a heat gun, stirring occasionally to ensure homogeneity. Once fully blended, the photo initiator BAPO at 1 wt % (0.30g,  $7.2 \times 10^{-4}$  mol) was added along with 10 or 15 % chitosan by weight relative to the total monomer and crosslinker weight and the vial was ultrasonicated (approximately 25 min). For the 10 wt % loading, 3g of the desired chitosan was added into the amber vial and for the 15 wt % loading, 4.5g of the desired chitosan was added.

## 2.3 3D Printing

All samples were printed using a Photon Mono 4K DLP 3D printer at 405 nm. The printed specimens for tensile testing were ASTM D638 standard specimen type IV. Once printed, unreacted excess resin was washed off using isopropanol followed by post-curing under a 405 nm lamp for 24 h.

## 2.4 Characterization of Chitosan Powders and Composites

Tensile tests were performed on ASTM D638 standard type IV with an Instron 6800, using a 500 N load cell. A 10 mm/min extension rate was applied to all samples until failure, with a minimum of four samples per formulation to obtain the stress-strain curves to determine the ultimate tensile strength (UTS), strain at break, Young's modulus, and toughness as averages with a standard deviation. Thermal characterization was performed using thermogravimetric analysis (TGA) on a Mettler Toledo SDT. 5-10 mg samples were loaded in an alumina crucible using a heating rate of  $10 \text{ }^\circ\text{C min}^{-1}$ , from 25 to  $700 \text{ }^\circ\text{C}$  under a nitrogen atmosphere (flow rate of  $100 \text{ mL min}^{-1}$ ). Fourier transform infrared spectroscopy (FTIR) was performed on a Cary 600 series using an attenuated total reflection apparatus at  $25 \text{ }^\circ\text{C}$  with a resolution of  $2 \text{ cm}^{-1}$ . Spectra were collected in the  $4000 - 400 \text{ cm}^{-1}$  range with 32 scans per sample. Powder X-ray diffraction (PXRD) was used to determine crystallinity of chitosans using a Bruker D8 diffractometer with a Cu ( $K\alpha$ ,  $\lambda = 0.154 \text{ nm}$ ) radiation source. Measurements were taken from  $2\theta$ ,  $2^\circ$  to  $30^\circ$ . Gel content and swelling tests were performed with square samples cut from the 3D printed parts. The initial weight of the samples was recorded, then they were placed in separate vials with either tetrahydrofuran (THF) or water for 24 h. The samples were dried and weighed to determine the percent swelling. The samples were then dried in a vacuum oven at  $80 \text{ }^\circ\text{C}$  for 24 h and the final weight was recorded. The gel content and swelling tests were done in triplicate to obtain averages and standard deviation. The surface morphology of the samples was evaluated by scanning electron microscopy (SEM). The images were obtained with a Zeiss SUPRA 40 scanning electron microscope (Carl Zeiss Microscopy). The samples were mounted on 15 mm aluminum stubs using double-sided adhesive copper tape.

## 3. Results and Discussion

### 3.1 Chitosan

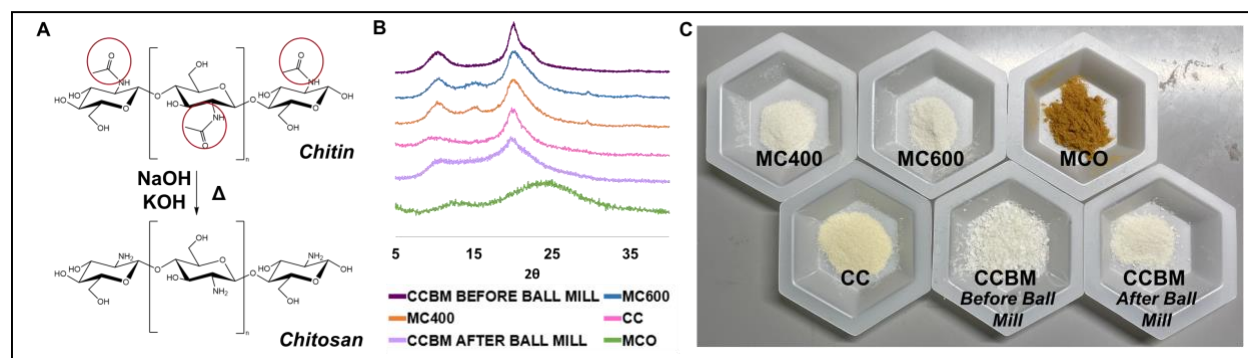


**Figure 1:** (A) Chitin can be converted to chitosan through deacetylation, which creates free amine functional groups that can participate in hydrogen bonding. (B) PXRDs of chitosan powders, with varying amounts of crystallinity. (C) Image of chitosan powders, with the comparison of the CCBM powder before and after the ball mill process.

To obtain chitosan, chitin must be deacetylated. This is done by placing chitin in an aqueous alkali solution and heating. The longer the product undergoes heat in solution, the greater the degree of deacetylation (DDA).<sup>18,21,22</sup> The deacetylation process will hydrolyze the acetamide group in chitin and produce the amino group seen in chitosan, as shown in **Figure 1A**. The greater the deacetylation, the greater number of free amino groups present in the chitosan. The presence of amino and hydroxyl groups in chitosan allows for the biopolymer to hydrogen bond with the monomers and crosslinkers within the photoresin.<sup>22,30,34</sup> Polydispersity, molecular weight, and DDA of the chitosan are the most influential parameters for the mechanical properties of chitosan composites.<sup>18,22</sup> In this work we use five different chitosan powders, sourced from either mushrooms (MC600, MC400, and MCO) or crustaceans (CC and CCBM), possessing a range of molecular weights, viscosities and DDAs, were selected for our composite resins (**Table 1** and **Figure S3**).

**Table 1:** Properties of the chitosans used for composite 3D photoprinting.

Chitosan	Source	Solubility	Molecular Weight (Da)	Viscosity (cps)	DDA
CCBM	Crab/Shrimp	Acid	85k	6	80 %
CC	Crab/Shrimp	Acid	190k-310k	494	88 %
MC400	Oyster mushroom	Acid	120k-700k	400	98 %
MC600	Oyster mushroom	Acid	700k-1500k	600	98 %
MCO	Oyster mushroom	Water	≤3000	≤ 5	98 %

PXRD data were collected for all chitosans to evaluate the degree of crystallinity, as shown in **Figure 1B**. We also observed the effects of using ball milling (CCBM) to break down the chitosan into fine powder form (**Figure S1** and **Figure S2**). PXRD patterns collected before and after BM show that this mechanical treatment decreases the crystallinity of the chitosan powder giving a more amorphous material, as observed by the reduction in peak sharpness after milling.<sup>17</sup> The CCBM particles could be blended into the matrix more effectively than its original flaky form. Chitosan powder colors and sizes can be seen in **Figure 1C**. Powder color and size can be seen in **Figure 1C**. In the FTIR spectra (**Figure S7**) we observe a reduction of intensity of the amine peaks (around 2300  $\text{cm}^{-1}$ ) from pre-ball milled chitosan to post-ball milling, indicating that the bonds have been changed or destroyed and there are less amines present in the new post-ball milled form.

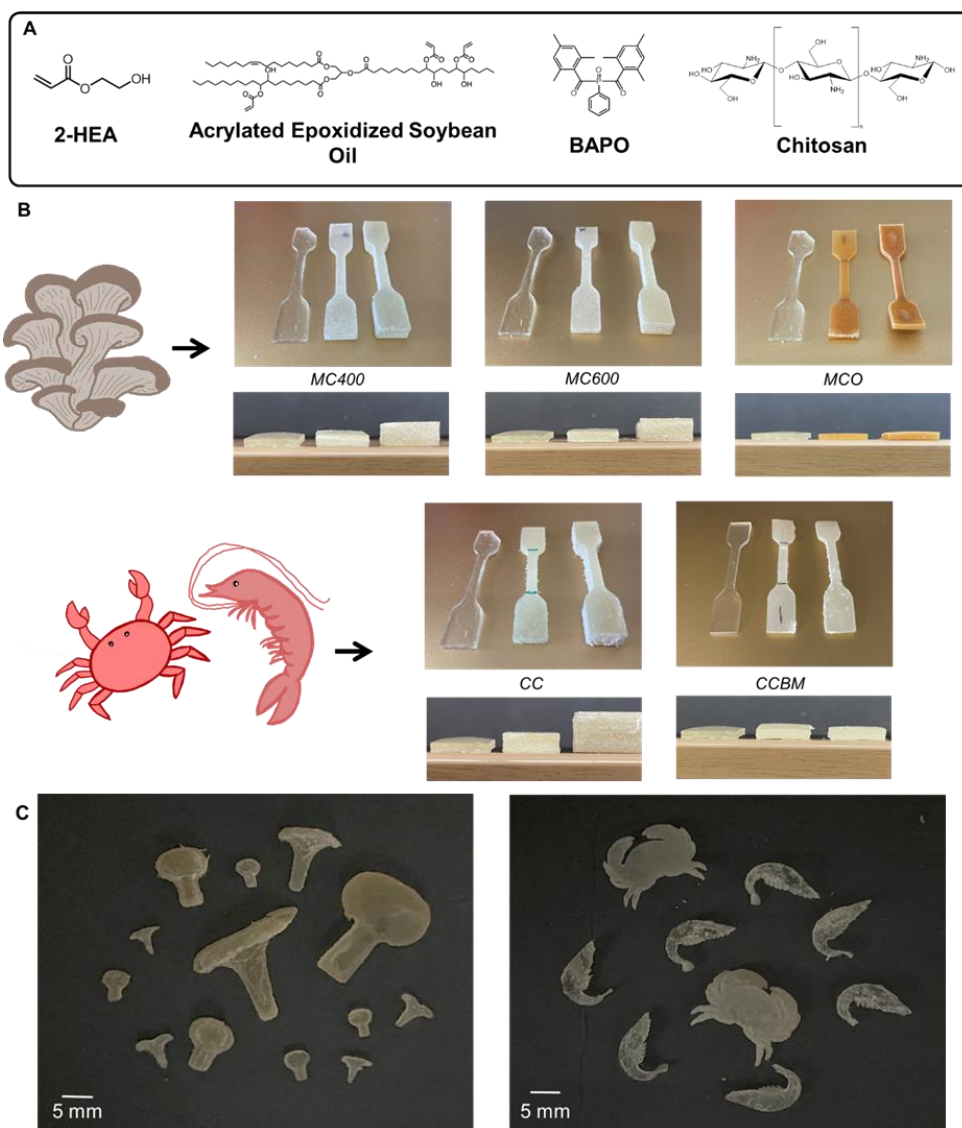


**Figure 2:** (A) Formulation for the chitosan composites, with variation in chitosan loading at either 10 or 15 weight %. (B) Example dogbones for each chitosan, showing the control, then 10 and 15 weight % from left to right for each composite. (C) Example 3D printed objects for mushroom chitosan (left) and crustacean chitosan (right).

**Table 2:** Percent increase of the print width as composite loading used increased for each print compared to the control.

	SAMPLE	WEIGHT (%)	THICKNESS (mm)	± SD	INCREASE (%)
	Control	0	1.94	0.05	
	CC	10	4.49	0.19	131
		15	8.55	0.15	341
	CCBM	10	2.72	0.22	40
		15	3.32	0.41	70
	MC400	10	3.46	0.14	78
		15	6.42	0.15	231
	MC600	10	3.25	0.10	68
		15	6.67	0.24	244
	MCO	10	2.11	0.07	9
		15	2.34	0.09	21

### 3.2 Chitosan Resins and 3D Printing

The resin was formulated to produce a viscosity that would enable homogenous incorporation of the chitosan without settling or separation during 3D printing. This was achieved by using a 75:25 ratio by weight of HEA:AESO (**Figure 2**). The AESO increases the viscosity of the print and reduces the need for the petroleum-based HEA component. Chitosan was incorporated at both 10 and 15 wt %, with higher loadings above 15 wt % being too viscous and opaque to be 3D printed. The morphology of the chitosan played a direct role in how well it can be blended into the photoresin. The CCBM chitosan was large and flaky before ball milling, and would not stay suspended in the photoresin, as seen in **Figure 1C**. After ball milling, the resulting fine powder form could be used to produce a uniform, and printable, composite photoresin (**Figure S1** and **Figure S2**). The particle sizes of all the mushroom chitosans are finer than either of the crustacean sourced chitosan (**Figure S3**). MC600 and MC400 particles can pass through an 80-mesh sieve, while the MCO particles can pass through a 100-mesh sieve. The finer particle sizes make the mushroom sourced chitosan easy to homogeneously suspend within the photoresin.

As the loading increased in the CC, MC400, and MC600 composite dogbones, we observe an increase in printed part thickness compared to the control (**Figure 2B** and **Table 2**). The greatest increase in thickness came from the CC-10 to CC-15 dogbones which increased by 131% to 341% with increasing chitosan composition. This is not the case for the MCO and CCBM composites, their increase in thickness is minimal as the particle sizes are reduced to under 50  $\mu\text{m}$ . The dogbone prints differ due to the increase in the composite particle size obstructing the light source and the interactions occurring between the composite and the photoresin matrix.

### 3.3 Evaluation of Mechanical Properties

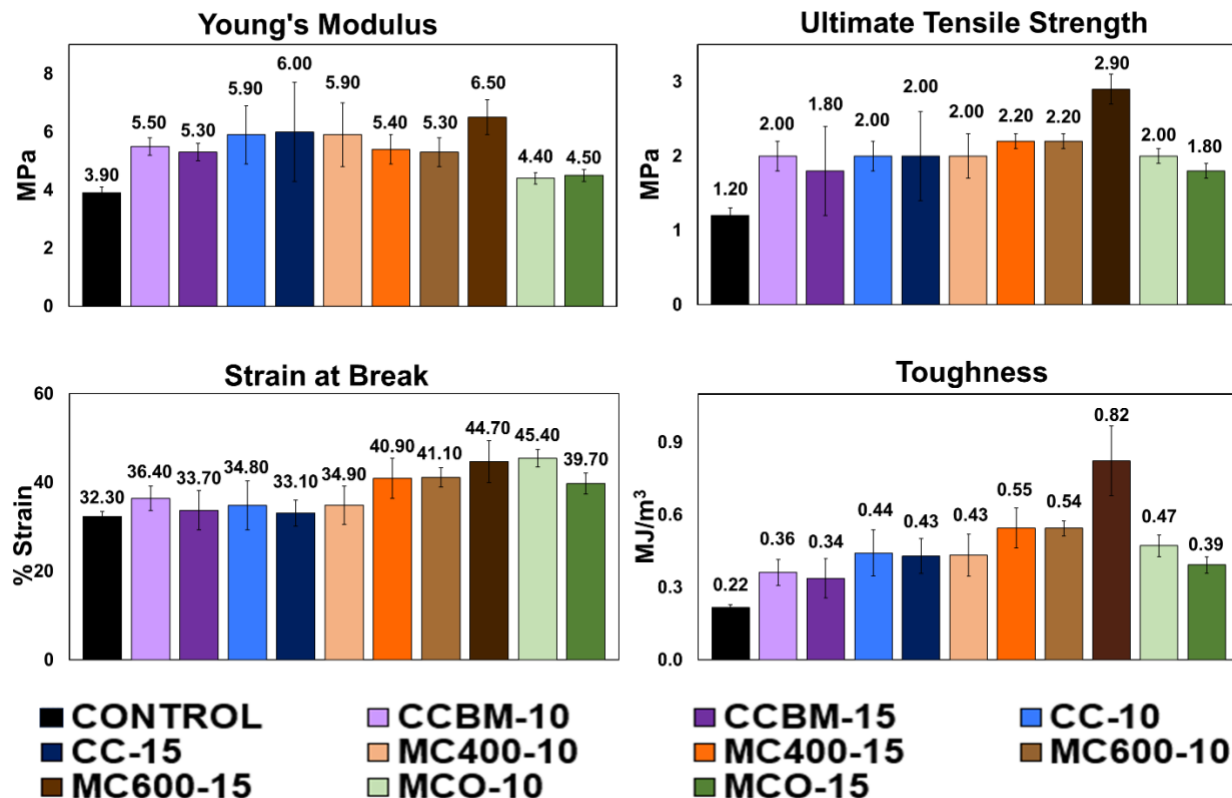


**Figure 3:** (A) Young's Modulus, (B) ultimate tensile strength, (C) strain at break, and (D) toughness of all printed specimens.

The mechanical properties of the chitosan composite and control prints were evaluated by tensile tests using 3D-printed dogbones as seen in **Figure 3** and **Figure S4**. The control sample (no chitosan additive) has an ultimate tensile strength (UTS) of 1.2 MPa (**Figure 3B**). All types of chitosan increased the UTS with MC600 having the greatest improvement to the resin strength. MC600-10 and MC600-15 increased in UTS by 1.8 to 1.4-fold respectively. The CC chitosan improved the strength of the printed polymers while loading percent increase made little to no difference for UTS with an average improvement of 1.7-fold. MCO and CCBM loaded dog bones improved the strength compared to the control. With higher loadings (greater than 10 weight percent) of chitosan in MCO and CCBM there is no significant change in strength. The higher molecular weight chitosan had a greater impact on the strength of the printed materials. The maximum tensile strength observed is for the MC600-15 which resulted in 2.9 ( $\pm 0.2$ ) MPa with an enhancement of 242% compared to the control.

All chitosan composites studied here demonstrated increased Young's modulus compared to the control (**Figure 3A**). The MC600 composite has the greatest capability to withstand changes in length and tension as the loading increased. With MC600-10 chitosan loading the YM is 5.3 ( $\pm 0.5$ ) MPa and MC600-15 increased to 6.5 ( $\pm 0.6$ ) MPa. Compared to the control, we see a stiffening of the material by 136% to 167% respectively. The strain at break values are reported

in **Figure 3C**. Both crustacean sourced chitosans have similar trends where higher loadings resulted in increased stiffness with concomitant reduced strain capacity. In contrast, MC400 and MC600 have increased strain capacity even as the filler loading was increased. The highest strain at break value was observed to be the MCO-10 print, with the value of 45.4% compared to the 32.3% strain at break of the control. In toughness (**Figure 3D**) the most improved sample is MC600-15 which increased almost four times compared to that of the control print sample. While all composite formulations improved in toughness, there was greater increase with MC400 and MC600.

The oligomer chitosan (MCO) plasticized the resin formulation, resulting in greater strain before breaking and the capability to revert back to its original shape after straining. While the MC600 showed increased improvement in UTS and strain with greater composite loading making the material stronger and more durable than the original resin material. This indicates that the crystalline structure and molecular weight of the chitosan play an important role in the mechanical properties of the resin formulation. We observe a trend between the crystallinity of the chitosan and the strength and flexibility of the polymer composites. Overall, the more crystalline chitosan fillers improved the UTS of the polymers while the less crystalline polymers generally improved in strain at break. In the CCBM sample, the crystalline structure is partially destroyed in the process which is reflected in the mechanical properties. The composite was unable to improve the mechanical properties to the degree of other chitosan counterparts. The same trend can be seen in the oligomer sample (MCO) which lacks in crystallinity.

The results after the incorporation of chitosan show how the 2-HEA/AESO matrix can successfully transfer stress to the chitosan filler as tension occurs. The presence of many amine groups and hydroxyl groups in the chitosan molecule provides hydrogen bonding interactions between the composite filler and photoresin matrix.<sup>35</sup> We observed an overall decrease in degree of swelling, suggesting non-covalent interactions between the photoresin matrix and the composite filler are present (**Figure S5**). In both water and THF the polymers swelled between 41 – 53%. The polymers swelled the greatest with the polar/aprotic THF compared to other solvents. We observed from the gel content that the polymer is not losing composite particles, and the materials are fully polymerized. The thermal stability of all chitosan printed materials exceeded the thermal stability of the control up to temperatures between 230 to 310°C before the degradation of the polymer began (**Figure S6**).

### 3.4 Hydrogen Bonding in FTIR

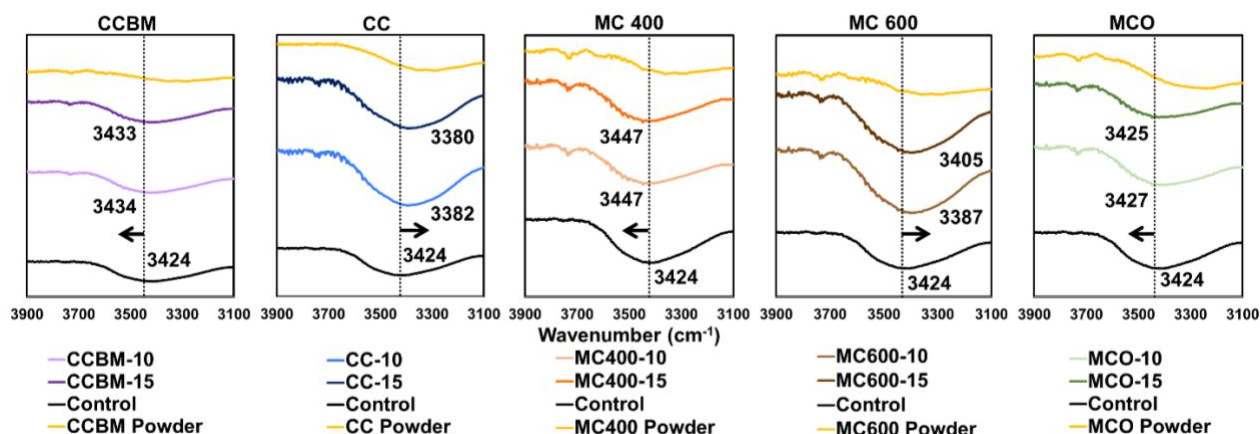


**Figure 4:** FTIR spectra of the hydroxyl and primary amine peaks for CCBM, CC, MC400, MC600, and MCO powders and print loadings compared to the control print including the shift taken by the composite filled prints.

The FTIR of the stretching of the primary amine and hydroxyl functional groups in the chitosan composite powders and their printed counterparts can be seen in **Figure 4**. There is red shifting occurring in the MCO, MC400, and CCBM chitosan composite print samples which indicates that there are hydrogen bonding interactions between the polymer matrix and the amino or hydroxyl groups of the chitosan. This red shift and increase in frequency show the hydrogen bonding length between the hydroxyl, amino, and carbonyl groups is increased. In the FTIR of the MC600 and CC printed composite samples, there is a blue shift in the amine and carbonyl signals at  $3423\text{ cm}^{-1}$  and  $1723\text{ cm}^{-1}$ , compared to the control print. This indicates that intermolecular forces are strengthened as the hydrogen bonding length is shortened.<sup>36,37</sup> The formation of intermolecular hydrogen bonding is observed between the hydroxyl and amine groups present in the chitosan and the hydroxyl and carbonyl groups present in 2-HEA and AESO.<sup>2,34,35</sup>

For higher viscosity and molecular weights, we observe a blue shift, while lower viscosity and molecular weight gave a red shift. The lengthening of the hydrogen bonds creates a weaker form of hydrogen bonding which is reflected in the mechanical properties of the MCO, MC400 and CCBM printed samples. We hypothesize the crystallinity, orientation, and chain arrangement of the chitosan affects the hydrogen bonding in the polymer matrix, giving us two different forms of shifting in the FTIR based on how the composite interacts with the photoresin.<sup>21</sup>

## 4. Conclusion

In this work, we created multiple chitosan composite photoresins that can be used in DLP 3D printers to print chitosan composite parts with loadings up to 15 wt %. The results after the incorporation of chitosan demonstrate how the 2-HEA/AESO matrix can successfully transfer stress to the chitosan filler. The mechanical properties, including the UTS, strain at break, toughness, Young's modulus, and thermal stability improved among all of the chitosan composite prints. There is an observable difference in the results based off the crystallinity and molecular

weight of each chitosan sample in the composite print, ultimately affecting the overall mechanical properties of the composite loaded photoresin. Our results show that the mushroom sourced chitosans are fully capable of producing similar if not better mechanical properties than crustacean sourced chitosans. Our future work in this area aims to create new resin formulations that can allow for higher chitosan composite loadings leading to greater options for sustainable cultivation, resource usage, improving biowaste issues, and reduced risk in allergy contaminations.

## Acknowledgements

We acknowledge the Welch Foundation (X-AT-0004-20230731) and the National Science Foundation (2323729) for support.

## References

- (1) Bagheri, A.; Jin, J. Photopolymerization in 3D Printing. *ACS Appl Polym Mater.* **2019**, 593–611. <https://doi.org/10.1021/acsapm.8b00165>.
- (2) Rajabi, M.; McConnell, M.; Cabral, J.; Ali, M. A. Chitosan Hydrogels in 3D Printing for Biomedical Applications. *Carbohydr. Polym.* **2021**, 260, 117768. <https://doi.org/10.1016/j.carbpol.2021.117768>
- (3) Zanon, M.; Cue-López, R.; Martínez-Campos, E.; Bosch, P.; Versace, D. L.; Hayek, H.; Garino, N.; Pirri, C. F.; Sangermano, M.; Chiappone, A. Bioderived Dyes-Mediated Vat Photopolymerization 3D Printing of Chitosan Hydrogels for Tissue Engineering. *Addit Manuf.*, **2023**, 69, 103553. <https://doi.org/10.1016/j.addma.2023.103553>
- (4) Cheng, Y. L.; Chen, F. Preparation and Characterization of Photocured Poly ( $\epsilon$ -Caprolactone) Diacrylate/Poly (Ethylene Glycol) Diacrylate/Chitosan for Photopolymerization-Type 3D Printing Tissue Engineering Scaffold Application. *Mater. Sci. Eng. C* **2017**, 81, 66–73. <https://doi.org/10.1016/j.msec.2017.07.025>.
- (5) Osi, A. R.; Zhang, H.; Chen, J.; Zhou, Y.; Wang, R.; Fu, J.; Müller-Buschbaum, P.; Zhong, Q. Three-Dimensional-Printable Thermo/Photo-Cross-Linked Methacrylated Chitosan-Gelatin Hydrogel Composites for Tissue Engineering. *ACS Appl Mater Interfaces.* **2021**, 13, 22902–22913. <https://doi.org/10.1021/acsami.1c01321>.
- (6) He, Y.; Wang, F.; Wang, X.; Zhang, J.; Wang, D.; Huang, X. A Photocurable Hybrid Chitosan/Acrylamide Bioink for DLP Based 3D Bioprinting. *Mater Des.* **2021**, 202, 109588. <https://doi.org/10.1016/j.matdes.2021.109588>.
- (7) Zhang, M.; Wan, T.; Fan, P.; Shi, K.; Chen, X.; Yang, H.; Liu, X.; Xu, W.; Zhou, Y. Photopolymerizable Chitosan Hydrogels with Improved Strength and 3D Printability. *Int J Biol Macromol* **2021**, 193, 109–116. <https://doi.org/10.1016/j.ijbiomac.2021.10.137>.

- (8) Vyas, A.; Garg, V.; Ghosh, S. B.; Bandyopadhyay-Ghosh, S. Photopolymerizable Resin-Based 3D Printed Biomedical Composites: Factors Affecting Resin Viscosity. *Mater Today Proc* **2022**, *62*, 1435–1439. <https://doi.org/10.1016/j.matpr.2022.01.172>.
- (9) Le Duigou, A.; Correa, D.; Ueda, M.; Matsuzaki, R.; Castro, M. A Review of 3D and 4D Printing of Natural Fibre Biocomposites. *Mater Des.* **2020**. 108911. <https://doi.org/10.1016/j.matdes.2020.108911>
- (10) Cortés-Guzmán, K. P.; Parikh, A. R.; Sparacin, M. L.; Remy, A. K.; Adegoke, L.; Chitrakar, C.; Ecker, M.; Voit, W. E.; Smaldone, R. A. Recyclable, Biobased Photoresins for 3D Printing Through Dynamic Imine Exchange. *ACS Sustain Chem Eng.* **2022**, *10*, 13091–13099. <https://doi.org/10.1021/acssuschemeng.2c03541>.
- (11) Johnson, R. M.; Cortés-Guzmán, K. P.; Perera, S. D.; Parikh, A. R.; Ganesh, V.; Voit, W. E.; Smaldone, R. A. Lignin-Based Covalent Adaptable Network Resins for Digital Light Projection 3D Printing. *J. of Polym Sci.* **2023**, *62*, 2585-2596. <https://doi.org/10.1002/pol.20230026>.
- (12) Perera, S. D.; Durand-Silva, A.; Remy, A. K.; Diwakara, S. D.; Smaldone, R. A. 3D Printing of Aramid Nanofiber Composites by Stereolithography. *ACS Appl Nano Mater.* **2022**, *5*, 13705–13710. <https://doi.org/10.1021/acsanm.1c03843>.
- (13) Parikh, A. R.; Cortés-Guzmán, K. P.; Bian, N.; Johnson, R. M.; Smaldone, R. A.; Lu, H.; Voit, W. E. Surface-Methacrylated Microcrystalline Cellulose Bioresins with Soybean Oil for Additive Manufacturing via Vat Photopolymerization. *J. Polym Sci* **2024**, *62*, 2692-2703. <https://doi.org/10.1002/pol.20230700>.
- (14) Piotrowska-Kirschling, A.; Brzeska, J. The Effect of Chitosan on the Chemical Structure, Morphology, and Selected Properties of Polyurethane/Chitosan Composites. *Polymers.* **2020**, *12*, 1205. <https://doi.org/10.3390/POLYM12051205>.
- (15) Miao, C.; Hamad, W. Y. Cellulose Reinforced Polymer Composites and Nanocomposites: A Critical Review. *Cellulose.* **2013**, *20*, 2221–2262. <https://doi.org/10.1007/s10570-013-0007-3>.
- (16) Grifoll-Romero, L.; Pascual, S.; Aragunde, H.; Biarnés, X.; Planas, A. Chitin Deacetylases: Structures, Specificities, and Biotech Applications. *Polymers.* **2018**, *10*, 352. <https://doi.org/10.3390/polym10040352>.
- (17) Podgorbunskikh, E.; Kuskov, T.; Rychkov, D.; Lomovskii, O.; Bychkov, A. Mechanical Amorphization of Chitosan with Different Molecular Weights. *Polymers (Basel)* **2022**, *14*, 4438. <https://doi.org/10.3390/polym14204438>.
- (18) Pellis, A.; Guebitz, G. M.; Nyanhongo, G. S. Chitosan: Sources, Processing and Modification Techniques. *Gels.* **2022**, *8*, 393. <https://doi.org/10.3390/gels8070393>.
- (19) Priyadarshi, R.; Rhim, J. W. Chitosan-Based Biodegradable Functional Films for Food Packaging Applications. *Innov Food Sci Emerg Technol.* **2020**, *62*, 102346. <https://doi.org/10.1016/j.ifset.2020.102346>.

- (20) Wittaya-Areekul, S.; Praharn, C. Development and in Vitro Evaluation of Chitosan-Polysaccharides Composite Wound Dressings. *Int J Pharm* **2006**, *313*, 123–128. <https://doi.org/10.1016/j.ijpharm.2006.01.027>.
- (21) Roberts, G. A. F. *Chitin Chemistry*; Macmillan Education UK, **1992**. <https://doi.org/10.1007/978-1-349-11545-7>.
- (22) Farinha, I.; Freitas, F. Chemically Modified Chitin, Chitosan, and Chitinous Polymers as Biomaterials. In *Handbook of Chitin and Chitosan: Volume 3: Chitin- and Chitosan-based Polymer Materials for Various Applications* **2020**, pp 43–69. <https://doi.org/10.1016/B978-0-12-817966-6.00002-9>.
- (23) Kim, H.; Kang, S.; Li, K.; Jung, D.; Park, K.; Lee, J. Preparation and Characterization of Various Chitin-Glucan Complexes Derived from White Button Mushroom Using a Deep Eutectic Solvent-Based Ecofriendly Method. *Int J Biol Macromol* **2021**, *169*, 122–129. <https://doi.org/10.1016/j.ijbiomac.2020.12.081>.
- (24) Pareek, N.; Vivekanand, V.; Agarwal, P.; Saroj, S.; Singh, R. P. Bioconversion to Chitosan: A Two Stage Process Employing Chitin Deacetylase from *Penicillium Oxalicum* SAEM-51. *Carbohydr Polym* **2013**, *96*, 417–425. <https://doi.org/10.1016/j.carbpol.2013.04.005>.
- (25) Mane, S.; Pathan, E.; Tupe, S.; Deshmukh, S.; Kale, D.; Ghormade, V.; Chaudhari, B.; Deshpande, M. Isolation and Characterization of Chitosans from Different Fungi with Special Emphasis on Zygomycetous Dimorphic Fungus *Benjaminiella Poitrasii*: Evaluation of Its Chitosan Nanoparticles for the Inhibition of Human Pathogenic Fungi. *Biomacromolecules* **2022**, *23*, 808–815. <https://doi.org/10.1021/acs.biomac.1c01248>.
- (26) Berger, L. R. R.; Stamford, T. C. M.; Stamford-Arnaud, T. M.; de Alcântara, S. R. C.; da Silva, A. C.; da Silva, A. M.; do Nascimento, A. E.; de Campos-Takaki, G. M. Green Conversion of Agroindustrial Wastes into Chitin and Chitosan by *Rhizopus Arrhizus* and *Cunninghamella Elegans* Strains. *Int J Mol Sci* **2014**, *15*, 9082–9102. <https://doi.org/10.3390/ijms15059082>.
- (27) Hoover, D. G. Production of Chitosan by Fungi. *Food Biotechnol* **1993**, *7*, 11–33. <https://doi.org/10.1080/08905439309549843>.
- (28) Kim, W. J.; Lee, W. G.; Theodore, K.; Chang, H. N. Optimization of Culture Conditions and Continuous Production of Chitosan by the Fungi, *Absidia Coerulea*. *Biotechnol. Bioprocess Eng.* **2001**, *6*, 6-10. <https://doi.org/10.1007/BF02942243>.
- (29) Elsacker, E.; Vandeloock, S.; Van Wylick, A.; Ruytinx, J.; De Laet, L.; Peeters, E. A Comprehensive Framework for the Production of Mycelium-Based Lignocellulosic Composites. *Sci Total Environ.* **2020**, *725*, 138431. <https://doi.org/10.1016/j.scitotenv.2020.138431>.
- (30) Shen, Y.; Tang, H.; Huang, X.; Hang, R.; Zhang, X.; Wang, Y.; Yao, X. DLP Printing Photocurable Chitosan to Build Bio-Constructs for Tissue Engineering. *Carbohydr Polym* **2020**, *235*, 115970. <https://doi.org/10.1016/j.carbpol.2020.115970>.

- (31) Seung, C. K.; Dalton, M. G.; Punt, A. E.; Poljak, D.; Foy, R. ECONOMIC IMPACTS of CHANGES in AN Alaska CRAB FISHERY from OCEAN ACIDIFICATION. *Clim Chang Econ (Singap)*. **2015**, *6*, 1550017. <https://doi.org/10.1142/S2010007815500177>.
- (32) Ghormade, V.; Pathan, E. K.; Deshpande, M. V. Can Fungi Compete with Marine Sources for Chitosan Production? *Int. J. Biol. Macromol.* **2017**, *104*, 1415–1421. <https://doi.org/10.1016/j.ijbiomac.2017.01.112>.
- (33) Zhang, S.; Chen, Z.; Wen, Q.; Yang, L.; Wang, W.; Zheng, J. Effectiveness of Bulking Agents for Co-Composting Penicillin Mycelial Dreg (PMD) and Sewage Sludge in Pilot-Scale System. *Environ Sci Pollut Res.* **2016**, *23*, 1362–1370. <https://doi.org/10.1007/s11356-015-5357-y>.
- (34) Dang, K. M.; Yoksan, R. Development of Thermoplastic Starch Blown Film by Incorporating Plasticized Chitosan. *Carbohydr Polym* **2015**, *115*, 575–581. <https://doi.org/10.1016/j.carbpol.2014.09.005>.
- (35) Husna, M. Y. N.; Chong, C. H.; Wong, V. L.; Cheah, K. H.; Wan, Y. K. 3D-Printed PEGDA Monolith with Robust Silane-Grafted Chitosan for Enhanced Textile Wastewater Treatment. *J Environ Chem Eng* **2022**, *10*, 108581. <https://doi.org/10.1016/j.jece.2022.108581>.
- (36) Joseph, J.; Jemmis, E. D. Red-, Blue-, or No-Shift in Hydrogen Bonds: A Unified Explanation. *J Am Chem Soc* **2007**, *129*, 4620–4632. <https://doi.org/10.1021/ja067545z>.
- (37) Pandey, P. Evidence of Blue-Shifting N-H...N Hydrogen Bonding despite Elongation of the N-H Bond. *RSC Adv* **2015**, *5*, 79661–79664. <https://doi.org/10.1039/c5ra17309d>.